Journal of Oil Palm Research
DOI: https://doi.org/10.21894/jopr.2025.0037

PHOTOCATALYTIC DEGRADATION OF ANAEROBIC TREATED PALM OIL MILL EFFLUENT BY MODIFIED ZnO WITH LEMONGRASS AND KINETIC STUDIES

DILAELEYANA ABU BAKAR SIDIK[1]*; NUR HANIS HAYATI HAIROM[2,3]; AIDA MUHAMMAD[1]; NORASIKIN OTHMAN[4,5]; NORELA JUSOH[4]; SITI FATIMAH MOHD NOOR[1]; HAFSA MOHAMMAD NOOR[1] and DZULHILMI KAMARUDIN SOHAMI[6]

ABSTRACT

The incorporation of green synthesis nanoparticles has a high photocatalytic degradation capability for treating anaerobic treated palm oil mill effluent (AnT-POME). Nevertheless, studies using zinc oxide-lemongrass nanoparticles (ZnO-L NPs) in photocatalytic processes for the treatment of AnT-POME are still in the early phases. Therefore, the goal of this study was to assess the photocatalytic degradation of AnT-POME in terms of colour, turbidity and chemical oxygen demand (COD) removal upon introducing modified ZnO-L NPs. The outcomes of this study demonstrate that the ideal conditions for photocatalytic degradation of AnT-POME have been established in the presence of ZnO-L NPs loading 0.1 g/L and pH 8, which results in a higher percentage of removal for colour (50.88%), turbidity (85.62%) and COD (97.02%). The photocatalytic process in the presence of ZnO-L NPs proved an improvement in colour, turbidity and COD removal when compared to without the addition of ZnO-L NPs. According to the experimental results, ZnO-L 1:3 NPs exhibit superior photodegradation of AnT-POME via pseudo first-order kinetics because of higher R^2 (0.9169) and K value (0.0167). Thus, the current study will gain a lot of attention because of the advantages of ZnO-L NPs' environmental performance in photocatalytic systems.

Keywords: anaerobic treated palm oil mill effluent, degradation, nanoparticles, photocatalytic.

Received: 27 September 2024**; Accepted:** 21 April 2025**; Published online:** 23 July 2025.

INTRODUCTION

The oil palm industry serves as one of the world's rapidly growing tropical sectors. Malaysia is presently regarded as the second-biggest exporter of palm oil after Indonesia because of its tropical environment and abundant natural resources. The problems associated with pollution brought on by palm oil mill effluent (POME) are getting worse as the palm oil business grows. POME contains a substantial number of organic compounds, that may negatively impact water quality and endanger both the environment and human health adversely (Sidik *et al.,* 2020). The secondary biological treatment of POME results in the production of anaerobic treated POME (AnT-POME). The breakdown of

[1] Centre for Diploma Studies,
Universiti Tun Hussein Onn Malaysia,
84600 Pagoh, Muar, Johor, Malaysia.

[2] Faculty of Engineering Technology,
Universiti Tun Hussein Onn Malaysia,
84600 Pagoh, Muar, Johor, Malaysia.

[3] Microelectronic and Nanotechnology - Shamsuddin Research Centre,
Faculty of Electrical and Electronic Engineering,
Universiti Tun Hussein Onn Malaysia,
86400 Parit Raja, Batu Pahat, Johor, Malaysia.

[4] Faculty of Chemical and Energy Engineering,
Universiti Teknologi Malaysia,
81310 Skudai, Johor, Malaysia.

[5] Centre of Lipids Engineering and Applied Research (CLEAR),
Ibnu Sina Institute for Scientific and Industrial Research,
Universiti Teknologi Malaysia,
81310 Skudai, Johor, Malaysia.

[6] BASF (Malaysia) Sdn. Bhd.,
47800 Petaling Jaya, Selangor, Malaysia.

* *Corresponding author e-mail: dila@uthm.edu.my*

lignocellulosic substances is responsible for AnT-POME's brownish colouration and elevated colour intensity (1,500 pt/Co). Additionally, AnT-POME has substantial concentrations of chemical oxygen demand (COD) (1,200 mg/L), turbidity (2,300 NTU), and total suspended solids (1,800 mg/L), all of which exceeded the Malaysian government's standard discharge guideline (Mohamad *et al.*, 2021; Muhamad *et al.*, 2022). Therefore, improper AnT-POME treatment could have a negative impact on water bodies and the environment.

Palm oil industries are currently utilising biological treatment, which has various problems, including the production of secondary pollutants (AnT-POME), which may have a severe environmental impact. Over 85.00% of milling companies in Malaysia generally use an open ponding method for POME treatment (Sayuti & Azoddein, 2015**)** and the Department of Environment (DOE) will enforce the requirements in accordance with the Environmental Quality Act of 1974 and palm oil mills are regulated under Environmental Quality (Prescribed Premises) (Crude Palm Oil) Regulations 1977. The safe limit for POME waste being released, referring to the DOE Malaysia, is established at 100 ppm of biological oxygen demand (BOD), and no regulation for COD concentration for palm oil mills (Muhamad *et al*., 2022; Razali *et al*., 2021). However, the current limit is generally complied by the mills using ponding system. Only those mills with BOD 20 ppm struggling to achieve consistently. In recent years, numerous technologies, and polishing techniques for AnT-POME have been established to enhance the performance of treated AnT-POME in accordance with the requirements of the DOE prior release to a water body.

In recent years there has been a significant rise in interest in alternative technologies for POME treatment. The foremost examples are the photocatalytic (Tan *et al.*, 2023), hybrid plasma and acoustic (Chan *et al.*, 2023), integrated photovoltaic-electrocoagulation (Mohamad *et al.*, 2022), coagulation-flocculation process (Lim *et al.*, 2022) and membrane technology (Som & Yahya, 2021). The drawbacks of the traditional open ponding approach are successfully addressed by the aforementioned solutions, which are efficient and practicable. Even though there are numerous cutting-edge technologies accessible from previously conducted studies, there are still several obstacles that prevent them from being used for POME treatments in industry. These obstacles include those related to cost, feasibility, performance and environmental impact. Even after numerous treatments, the POME's characteristics still do not meet the DOE's standards for discharged materials since the levels of COD, BOD and colour intensity are still excessive and considered dangerous to discharge.

The photocatalytic process, which uses the notion of advanced oxidation processes (AOPs), that is associated with the transfer of electrons in the degradation of organic matter, has become another viable advanced wastewater treatment for POME (Moksin *et al.*, 2021; Puasa *et al.*, 2021). Theoretically, the mechanism of the photocatalytic degradation process begins with a photoexcitation stage that occurs when electrons (e) in the valence band (VB) are excited to the conduction band (CB), producing positively charged holes (h^+). Then, as h^+ and e are formed in the system, the hydroxyl radical (•OH) is created. This radical (•OH) is essential for the breakdown of organic matter pollutants into simple molecules like methane (CH_4), carbon dioxide (CO_2), water (H_2O) and other compounds (Chin *et al.*, 2022). Generally, photocatalysts are crucial for the efficiency of the photocatalytic process in producing good-quality treated wastewater (Puasa *et al.*, 2021). Additionally, Ren *et al.* (2023) asserted that photocatalytic degradation is one of the promising techniques since it can totally mineralise organic pollutants under simple circumstances like ambient temperature and pressure. Aside from that, according to Chin *et al.* (2022) the advantages of the photocatalysts used in the photocatalytic system include their ability to be recycled or reused and yet still maintain the degrading efficiency. The photocatalytic degradation process is therefore the most pertinent method to treat AnT-POME out of all those mentioned previously. Consequently, this study suggests photocatalytic degradation as one of the promising strategies.

The development of highly efficient semiconductors, such as titanium dioxide (TiO_2), zinc oxide (ZnO), cadmium sulfide (CdS), tin dioxide (SnO_2), Copper (II) oxide (CuO), tungsten trioxide (WO_3), iron (III) oxide (Fe_2O_3), strontium titanate ($SrTiO_3$), cerium dioxide (CeO_2) and calcium oxide (CaO), has been the subject of numerous studies to date (Chin *et al.*, 2022; Ren *et al.*, 2023). ZnO has been recognised as a notable photocatalytic material due to its environmental compatibility, cost-effectiveness and excellent photocatalytic efficiency (Ng *et al.*, 2019; Shkir *et al.*, 2024d). Furthermore, ZnO has also received a lot of attention for its photocatalytic potential due to its advantageous properties, which include strong excitation binding energy, a substantial surface area, high reactivity, biodegradable, photosensitivity and higher stability (Chin *et al.*, 2022; Ng *et al.*, 2019; Shkir *et al.*, 2024c).

The surface morphology of ZnO has been improved by several methods including doping with suitable transition elements enables tuning its properties, making it suitable for many applications (Alagarasan *et al.*, 2024; Jansi *et al.*, 2024; Khan *et al.*, 2024; Shkir *et al.*, 2024d). The particle size and morphology of nanoparticles can also be enhanced

to promote efficient photocatalytic application by adding capping agents such as polyvinylpyrrolidone (PVP) (Hairom *et al.*, 2015), polyethylene-glycol (PEG) (Desa *et al.*, 2020) and plant-based extracts (Shkir *et al.*, 2022a) during the formation of ZnO nanoparticles. An additional surfactant called a capping agent is utilised to prevent specific nanoparticles from aggregating and to hinder their growth (Agarwal *et al.*, 2017). Importantly, the capping agent can affect the structural properties of nanoparticles in surface engineering, including their size and shape. Lemongrass leaves are useful as a capping agent since they are simple to get, affordable and environmentally-friendly. Previous studies on the biosynthesis of ZnO photocatalyst demonstrated ZnO's adaptability as a photocatalyst that can degrade a significant number of organic materials for various types of wastewaters (Rao *et al.*, 2022; Sayadi *et al.*, 2022).

Sidik *et al.* (2020) have demonstrated the efficacy of a hybrid photocatalytic membrane reactor system in treating palm oil mill secondary effluent (POMSE). Nonetheless, the biggest obstacle to the application of membranes in wastewater treatment is their frequent replacement requirement, which might increase maintenance and operational costs. In addition, the usage of ZnO-L NPs in a photocatalytic system alone is still regarded as new. As a result, the current work intends to investigate the efficacy of ZnO-L NPs in AnT-POME treatment utilising the photocatalytic system to fill the gap of membrane fouling concerns employing a membrane system.

MATERIALS AND METHODS

Materials

The AnT-POME sample was collected in an airtight container from a neighbouring palm oil plantation's open pond in Pagoh, Johor, Malaysia. APHA 2012 standard techniques were used to analyse the original AnT-POME characteristics such as pH, COD, turbidity and colour. The AnT-POME samples were stored at 4°C in a chiller before being used. R&M Marketing, Essex, UK, provided commercial ZnO (Sigma-Aldrich). In the meantime, BT Scientific, Malaysia supplied the hydrochloric acid (HCl) and sodium hydroxide (NaOH) that were used to modify the pH of the AnT-POME solution.

Green Synthesis of ZnO–L NPs

Ten g of powdered form of dried lemongrass leaves were heated with 100 mL of deionised water for 2 hr at 80°C. The lemongrass solution was subsequently filtered using filter paper (Brand: Whatmann No. 1). The filtrate was used to synthesise ZnO-L NPs in accordance with the previous protocol of Sidik *et al.* (2020). The precipitation method involved the addition of 0.10 M zinc acetate, 0.15 M oxalic acid and lemongrass leaves extract based on various ratios of ZnO solution to lemongrass leaves extract (1:3 and 1:9). A magnetic stirrer was used to vigorously stir the mixture for 24 hr. The precipitated material was then filtered from the mixture and dried in an oven at 100°C for 1 hr. Upon synthesising, the extracted material was calcined in a furnace for 2 hr at 500°C. Fourier transform infrared spectrophotometer (FTIR Model; Agilent Tech Cary), field-emission scanning electron microscopy (FESEM Model; JEOL-JSM 7600F) and energy dispersive X-ray analysis (EDS) were used to characterise the ZnO-L NPs.

Photocatalytic AnT-POME by Modified ZnO-L NPs

Various parameters influencing the photocatalytic activity of the ZnO-L NPs were examined during the photocatalytic degradation process of AnT-POME. First and foremost, the photocatalytic procedure was carried out utilising a technique established by Puasa *et al.* (2021) using different ZnO-L NPs (1:3 and 1:9), commercial ZnO and without ZnO under pH 8, AnT-POME initial concentration of 50% and photocatalyst loading of 0.1 g/L. *Figure 1* depicts the schematic diagram of the photocatalytic process at the laboratory scale that was used in this study. The photocatalytic process of AnT-POME was carried out in a 2.0 L reactor with an ultraviolet (UV) lamp and ZnO-L NPs. The light source was a UV lamp that emitted mostly at 253.7 nm and had a defined power of 18 W. Before beginning the photocatalysis procedure, the mixture was rigorously stirred using an impeller (PL111) with an overhead stirrer (WireStir HS-30D) at 150 rpm in the dark for 30 min to achieve photocatalyst adsorption-desorption equilibrium. A water chiller was used to circulate cooling water throughout the process, keeping the temperature at ambient (25°C) levels. At intervals of 10 min, approximately 5.0 mL of the sample was taken out of the reactor for COD analysis. The whole process was repeated by using a different photocatalyst loading (0.1, 0.3 and 0.5 g/L) and pH (4, 6 and 8) to determine the best operating condition for the photocatalytic process. To prevent contamination, the photocatalytic treated effluent was collected and kept at 4°C before the performance study.

Analytical Method

The treated AnT-POME samples were separated by using a centrifuge for 20 min at 8,000 rpm under 4°C. The treated AnT-POME samples were analysed in terms of colour intensity, COD, turbidity and

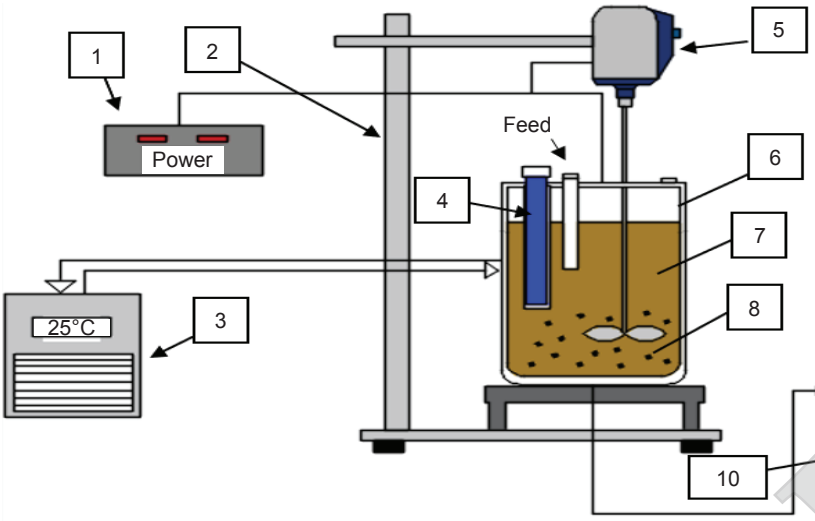

Note: 1 - Power source; 2 - Retort stand; 3 - Water chiller, 4 - UV lamp; 5 - Overhead stirrer, 6 - Photocatalytic reactor; 7 - AnT-POME; 8 - ZnO-L NPs; 9 - Valve; 10 - Measuring cylinder.

Figure 1. Schematic diagram of the photocatalytic reactor.

pH. According to the ADMI standard procedure (Program: 97 Color ADMI 1 inch), the colour intensity was measured using a DR6000 UV-Vis Laboratory Spectrophotometer (Model: Hach). The treated AnT-POME (2 mL) was added into COD digestion reagent vials then was inserted into the preheat DRB200 (Hach, Germany) reactor and heated at 150°C for 2 hr. The sample was then cooled to room temperature before further analysis using the DR6000 Spectrophotometer. The turbidity was determined via a portable turbidity meter (Model: Cole Parmer Oakton) and pH was measured using a portable pH meter (Milwaukee). The percentage of removal was calculated according to Equation (1) (Sidik *et al.*, 2020).

$$\text{Removal}\ (\%) = \frac{(C_0 - C_t)}{(C_0 \times 100)} \quad (1)$$

where, C_0 and C_t denote the colour intensity, COD and turbidity at time zero and at time (t), respectively.

Kinetic Study of Photocatalytic AnT-POME

The photocatalytic activity of AnT-POME in the presence of ZnO-L NPs was established via a pseudo-first-order kinetic model according to the Langmuir-Hinshelwood (L-H) rate law [Equation (2)].

$$-\frac{dC_A}{dt} = (-r_A) = \frac{kC_A}{1 + K_A C_A} \quad (2)$$

It is possible to further simplify the expression for the denominator to ($1 >> K_A\ C_A$) ≈ 1 at low reactant concentrations, reflected in this investigation by the organic content of the AnT-POME. As a result, a single Power Law model may easily explain the AnT-POME decomposition behaviour. The batch photocatalytic kinetics that adheres to the pseudo-first-order reaction kinetics is as shown in Equation (3).

$$-\frac{dC_A}{dt} = kC_A \quad (3)$$

The expression shown in Equation (4) is obtained by integrating Equation (3):

$$\text{Ln}\left(\frac{C}{C_O}\right) = kt \quad (4)$$

where C_O is the starting COD concentration (*mg/L*), *C* is the COD concentration at time (mg/L), t is the time (min), and *k* is the apparent specific response time (min^{-1}). The particular reaction time, *k*, for each experiment, as well as the R^2 values, will be established by plotting a graph of Ln $\left(\frac{C}{C_O}\right)$ *vs.* time (Schnabel *et al.*, 2022).

RESULTS AND DISCUSSION

Characterisation of ZnO-L NPs

As shown in *Figure 2a*, FTIR spectroscopy was used to demonstrate the functional groups composition presence in ZnO-L 1:3 NPs within the 400-6,000 cm^{-1} infrared adsorption band. According to *Figure 2a*, the structures of the O-H

groups that define the polysaccharides from lemongrass leaves had a vibration frequency of 3,390.199 cm^{-1}. This phenomenon might be brought on by some biomolecules that were isolated from lemongrass leaves, like phenolic compounds. In accordance with Ajayi and Afolayan (2017) and Devi *et al*. (2016), the protein's aromatic stretching of -C-N, which serves as both a capping and a reducing agent, is the cause of the extremely strong absorption peak at 1,444.402 cm^{-1}. Based on Sidhu *et al.* (2022), the amide bond and aromatic ring both played a role in the production of the metal nanoparticles and could serve as their capping agents. The function of amide bonds and aromatic rings as capping agents is attributed to their distinctive chemical structures. Amide bonds possess strong conjugative effects and hydrogen bonding capabilities, which significantly enhance the stability of materials. Meanwhile, the π-π stacking interactions inherent in aromatic rings facilitate robust intermolecular interactions at interfaces, thereby augmenting the material's physicochemical properties (Cao *et al.*, 2024; Shi *et al.*, 2020a; 2020c).

The tiny particles were seen to be well-shaped. The FESEM image (*Figure 2b*) revealed aggregates of particles, and the aggregation may have been caused by the ZnO-L NPs' high surface energy. According to the TEM images (*Figure 2c*), the ZnO-L NPs 1:3 observed in this investigation are agglomerates with a hexagonal and spherical structure, having an average particle size between 20 and 60 nm. The results of the elemental analysis using EDX spectroscopy are shown in *Figure 2d*. A qualitative and quantitative status of the elements that might have been involved in the creation of ZnO-L NPs is provided by EDX analysis. Carbon, oxygen and zinc are the three elements that make up the synthesised ZnO-L NPs. Strong signals for zinc and oxygen in the ZnO-L NPs show that ZnO NPs are formed.

Effect on Different Types of ZnO in Photocatalytic

In order to improve the photocatalytic performance, it is critical to investigate the ideal amount of photocatalyst used in the process. From an economic perspective, this is also a crucial criterion. The inclusion of ZnO-L NPs in the photocatalytic process allows the pigment particles in AnT-POME to be degraded, resulting in lower colour intensity, turbidity and COD.

Photocatalytic activity may vary depending on the catalyst's surface or characteristics, which impact pollutant adsorption and electron-hole pair rate. Thus, it is critical to understand the impacts of various photocatalysts, such as ZnO-L 1:3 NPs,

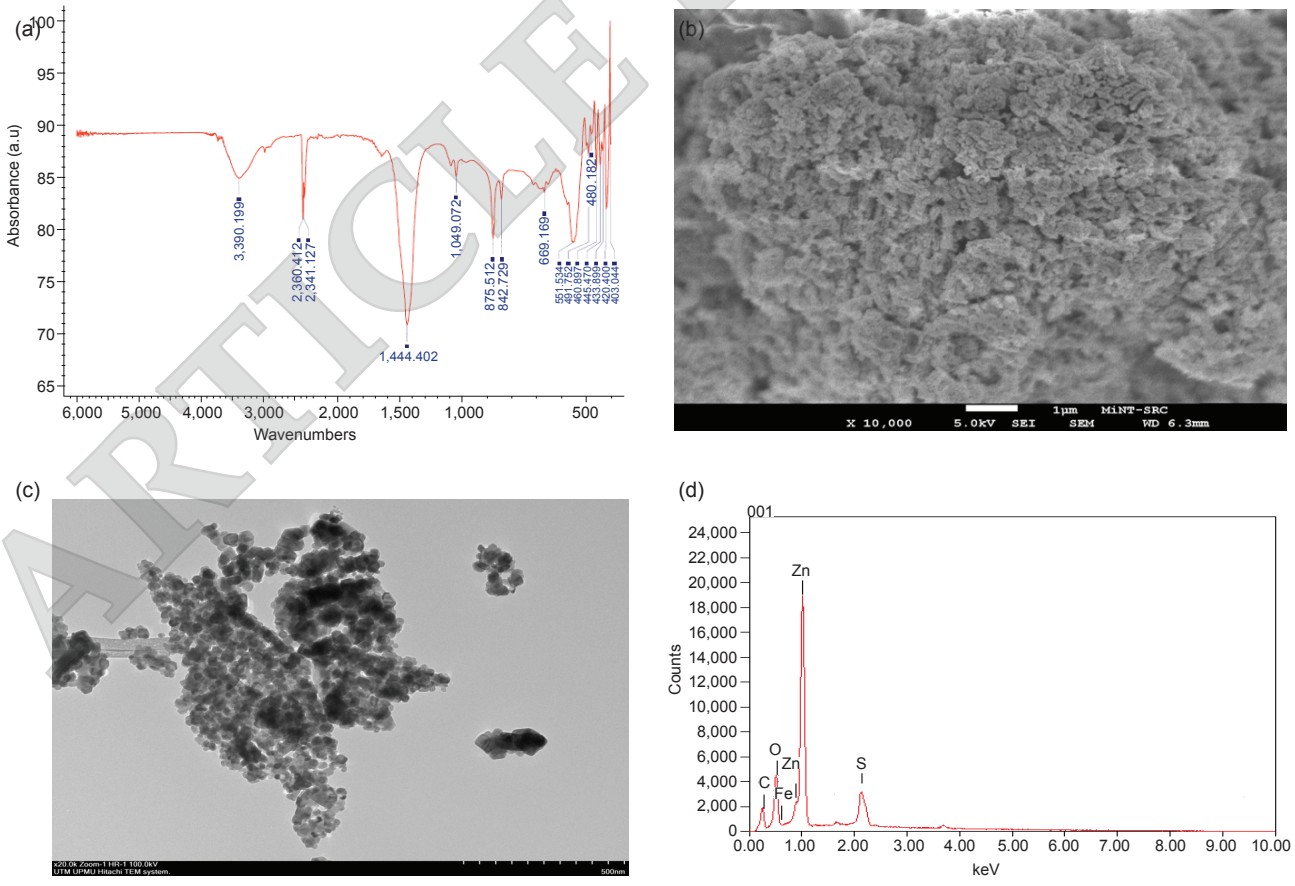

Figure 2. Characterisation of ZnO-L 1:3 NPs utilising (a) FTIR spectrum, (b) FESEM image, (c) TEM image and (d) EDX profile.

ZnO-L 1:9 NPs, without ZnO and commercial ZnO, on the decolourisation and degradation of AnT, as demonstrated in this study. In comparison to ZnO-L 1:9 NPs, without ZnO and commercial ZnO, *Table 1* demonstrates that treated AnT-POME in the occurrence of ZnO-L 1:3 NPs has the best performance in terms of colour, turbidity and COD value. The colour intensity of AnT-POME that was treated using ZnO-L 1:3 NPs was 573.6 ADMI after undergoing photocatalytic treatment for 60 min. The value still surpasses the usual DOE criterion, which is that it must be less than 200.0 ADMI (Bello & Raman, 2017). Previous studies utilising various types of photocatalysts, such as ZnO-Clay (Awang *et al*., 2024), TiO_2 (Nawaz *et al*., 2020), and ZnO-PEG (Zainuri *et al*., 2018), have similarly encountered issues with the colour removal efficiency of AnT-POME. In order to diminish the colour till it reaches the specified value, AnT-POME must still undergo tertiary treatment.

Furthermore, the COD value obtained in the presence of ZnO-L 1:3 NPs is 20.3 mg/L lower than the minimum requirements set by DOE (50.0 mg/L) (Muhamad *et al*., 2022). Turbidity data for ZnO-L 1:3 NPs show the lowest value when compared to ZnO-L 1:9 NPs, commercial ZnO, and no ZnO are present. The fact that COD values were greater when no catalyst was introduced indicates that only a small quantity of the pollutant was broken down, demonstrating that the pollutant's molecular structure was stable and challenging to eliminate (Shi *et al*., 2020d). According to these findings, ZnO-L 1:3 NPs are thought to be the most efficient photocatalyst for treating AnT-POME through the photocatalytic treatment technique. This result can be explained by the tiny well-shaped ZnO-L 1:3 NP particles that were discussed in the previous section.

Figure 3a demonstrates that following photocatalytic treatment, the greatest COD elimination percentage is 97.02% at 0.1 g/L loading of ZnO-L 1:3 NPs. The proportion of COD removed from the treated AnT-POME without ZnO and commercial ZnO is 72.62% and 70.62%, respectively. This high COD removal from ZnO-L NPs may be attributed to the green synthesis capping agent's increased ability to stabilise nanoparticles and break down organic compounds in AnT-POME, which in turn improves photocatalytic performance. It is evident that the presence of ZnO-L 1:3 NPs resulted in a higher percentage of colour and turbidity removal compared to ZnO-L 1:9 NPs, commercial ZnO and without ZnO. As a result, the AnT-POME was treated with green ZnO-L NPs, which improved AnT-POME performance.

Photocatalysis is a surface-oriented process involving the adsorption of organic contaminants in the form of COD on the surface of ZnO NPs. *Figure 3b* shows the outcomes of an experiment in which the contact time for various types of ZnO was varied in order to determine the effect of contact time on COD removal AnT-POME. The graph clearly shows that COD elimination percentages improved significantly when the contact duration was increased from 10-90 min, reaching a maximum of 97.02%. The COD removal (%) capacity was sluggish from 30-90 min. It is beneficial to use modified green ZnO-L 1:3 NPs to increase the adsorption of AnT-POME contaminants on the photocatalyst surface, resulting in greater interaction between the pollutants and the catalyst. As a result, more pollutants can be degraded, increasing COD removal after 30 min.

Effect on Different Loading of ZnO-L NPs in Photocatalytic

The performance of the photocatalytic process is significantly influenced by the impact of various loadings of photocatalyst. The total photo-degradation process is greatly influenced by the number of ZnO-L NPs required to initiate a photocatalytic reaction, and the concentration of ZnO-L NPs is also crucial for developing a genuinely heterogeneous photocatalytic system. Following photocatalytic treatment, the treated AnT-POME from various ZnO-L NPs loadings (0.1, 0.3 and 0.5 g/L) are shown in *Table 2*. After 60 min of treatment, it was discovered that ZnO-L NPs with a loading of 0.1 g/L produced the best results, 573.6 ADMI for colour, 4.2 NTU for turbidity and 20.3 mg/L for COD were reported.

The proportion of COD, colour and turbidity removal from treated AnT-POME is shown in *Figure 4*. After the photocatalytic process, the small variation in AnT-POME percentage for colour removal is negligible. Increased photocatalyst loading boosts photocatalytic activity, however once a saturation phase is reached, it causes cloudiness in

TABLE 1. CHARACTERISTIC OF UNTREATED AND TREATED AnT-POME UNDER DIFFERENT TYPES OF ZnO

Parameter	Unit	Untreated AnT-POME	Type of ZnO NPs			
			Without ZnO	Commercial ZnO	ZnO-L NPs 1:3	ZnO-L NPs 1:9
Colour	ADMI	1,168.00	605.33 ± 0.47	607.33 ± 0.47	573.67 ± 0.47	612.67 ± 0.47
Turbidity	NTU	29.20	10.56 ± 0.01	14.65 ± 0.13	4.20 ± 0.10	9.32 ± 0.08
COD	mg/L	683.00	211.00 ± 0.00	200.67 ± 0.47	20.33 ± 0.47	192.67 ± 0.47

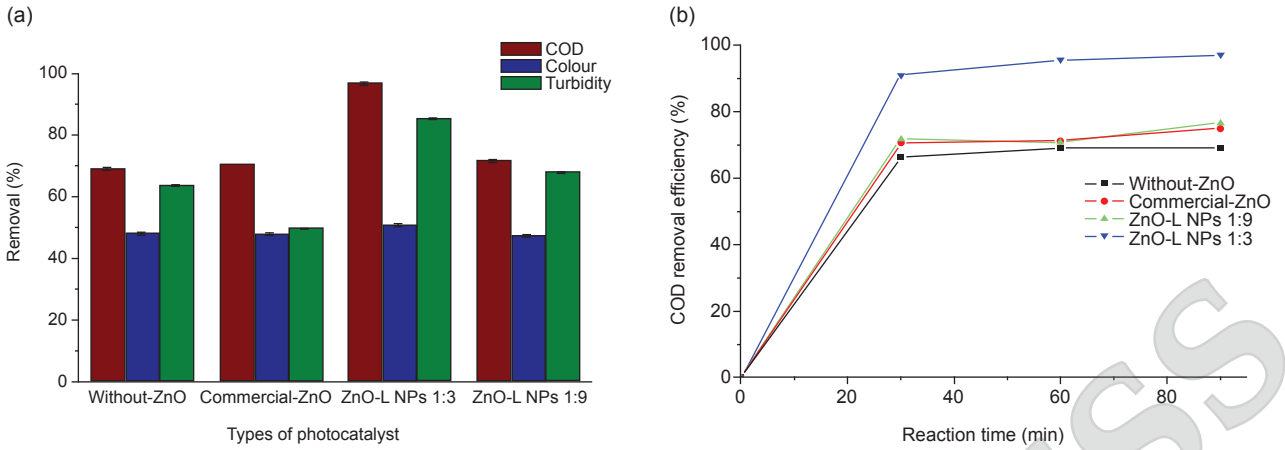

Figure 3. (a) Removal percentage of treated AnT-POME and (b) COD removal efficiency over reaction time using different types of photocatalyst.

TABLE 2. CHARACTERISTIC OF TREATED AnT-POME UNDER DIFFERENT LOADING OF ZnO-L (1:3) NPS

Parameter	Unit	Untreated AnT-POME	Different loading of ZnO-L NPs		
			0.1	0.3	0.5
Colour	ADMI	1,168.00	573.67 ± 0.58	602.00 ± 0.00	600.33 ± 0.58
Turbidity	NTU	29.20	4.20 ± 0.12	7.88 ± 0.13	5.27 ± 0.02
COD	mg/L	683.00	20.33 ± 0.58	217.33 ± 0.58	250.00 ± 0.00

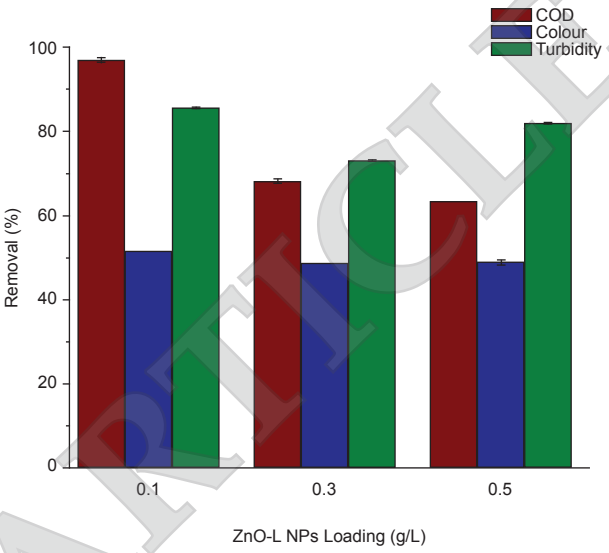

Figure 4. Percentage of treated AnT-POME from different loading of ZnO-L NPs.

the AnT-POME. Additionally, as shown in *Figure 4*, the percentage turbidity removal trend and colour removal trend are similar. The maximum rate of turbidity reduction, 85.62%, is demonstrated by ZnO-L NPs with a loading of 0.1 g/L. This may be due to the fact that a small concentration of ZnO-L NPs had an impact on the percentage of turbidity removal. While ZnO-L NPs loading of 0.3 and 0.5 g/L results in turbidity removal percentages of 73.03% and 81.96%, respectively.

The COD removal percentage trend indicates that the maximum COD reduction of 97.08% for AnT-POME was achieved at 0.1 g/L of ZnO-L NPs. Meanwhile, the COD percentage removal of the treated AnT-POME decreased significantly as the loading increased. One possibility is that the smaller size of ZnO-L NPs' results in higher surface areas for UV light absorption. Thus, for light to enter and degrade the organic molecules in AnT-POME, a lower catalyst concentration is preferred, leading to a higher COD removal.

Effect on Different pH

In the heterogeneous photocatalytic process, the impact of pH has a major impact on the efficiency of photocatalytic degradation. The AnT-POME sample was tested at different pH levels of 4, 6 and 8. Following a 60 min photocatalytic process, *Table 3* shows the results of treated AnT-POME at various pH levels, while *Figure 5* depicts the pattern of colour, turbidity and COD removal, respectively.

According to the data, the photocatalytic process of AnT-POME at pH 6 has the lowest reading of the colour value, which is 551 ADMI, and demonstrates

TABLE 3. CHARACTERISTIC OF TREATED AnT-POME UNDER DIFFERENT pH CONDITIONS

Parameter	Unit	Untreated AnT-POME	Different pH conditions		
			4	6	8
Colour	ADMI	1,168.00	568.67 ± 0.58	550.67 ± 0.58	573.67 ± 0.58
Turbidity	NTU	29.20	3.41 ± 0.20	2.89 ± 0.08	4.20 ± 0.12
COD	mg/L	683.00	255.00 ± 1.00	209.67 ± 1.15	20.33 ± 0.58

the largest proportion of colour degradation, which is 52.83%, in comparison to pH 4 and pH 8, where colour degradation is 51.28% and 50.88% respectively. The photocatalytic process with pH 6 also has the best turbidity reduction (90.11%) compared to pH 4 and pH 8, which had 88.32% and 85.62% reductions, respectively. The increased trend of removal at pH 6 may be caused by more ZnO-L NPs surface area available for UV light absorption, which will accelerate the photocatalytic process's degradation.

The tendency of pollutants in AnT-POME to aggregate under acidic conditions reduces the amount of active photocatalyst surface sites available for UV light to start the adsorption process, which may be the reason that acidic conditions cause less degradation. As a result, this barrier might slow down photocatalytic degradation and boost AnT-POME's colour intensity. The maximum COD elimination (97.02%) at pH 8 may be attributed to the more hydroxyl groups present in the basic state, which are able to breakdown more organic pollutants in AnT-POME. However, the presence of hydroxyl ions in base conditions above a particular limit may reduce colour removal. This behaviour might be caused by the competing molecule interfering with the photocatalytic breakdown of AnT-POME pigment.

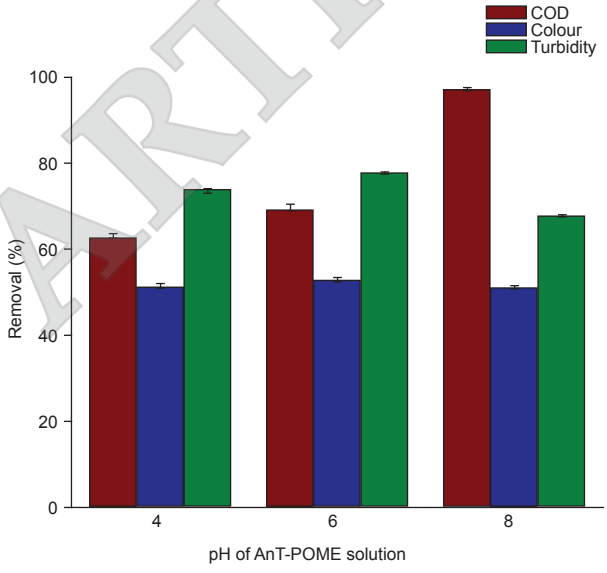

Figure 5. Removal percentage of AnT-POME under different pH.

Kinetic Study of Photocatalytic AnT-POME

Photocatalysis is the term used to describe the photoreaction-based pollutant degradation process that occurs on the ZnO-L photocatalyst surface. The process of degradation may differ depending on the type of pollutants and the organic materials they include. AnT-POME degradation kinetic models were evaluated for various photocatalyst types, ZnO-L NPs loading (0.1, 0.3 and 0.5 g/L), and pH (4, 6 and 8). A 60 min contact time was used throughout the entire experiment. As shown in *Figure 6*, the graph between $\left(\frac{C}{C_o}\right)$ and time exhibits a linear pattern with pseudo-first-order kinetics for different conditions in photocatalytic degradation of AnT-POME. The correlation coefficient (R^2) and rate of constant value (K) were calculated and presented in *Figure 6*.

The experimental findings with R^2 greater than 0.90 for each condition significantly suited the Langmuir-Hinshelwood model. The R^2 of commercial ZnO and ZnO-L 1:3 NPs were greater than 0.90, indicating that the photodegradation of AnT-POME followed the pseudo-first-order kinetics better than ZnO-L NPs 1:9 and without ZnO. However, the higher K, for various ZnO applications reveals that ZnO-L NPs 1:3 (0.0167) degrade at a faster rate than commercial ZnO (0.0034) conditions. As evidenced by the results, ZnO-L NPs exhibit greater photocatalytic activity.

The R^2 (0.9172) and K (0.0167) values are maximum at 0.1 g/L loading. Meanwhile, at 0.3 and 0.5 g/L loading of ZnO-L, the R^2 and K values decline. This result is supported by the higher removal of COD, colour and turbidity for 0.1 g/L ZnO-L loading as mentioned in the previous section. The shortage of a binding area found in ZnO-L photocatalyst causes the AnT-POME degradation efficiency to decrease with increasing loading. As a result, the optimal loading of ZnO-L NPs of 0.1 g/L was obtained in order to assess the future experimental process in large-scale applications to treat AnT-POME.

It is evident that as the pH rises from 6-8, the photocatalytic degradation increases. In fact, the maximum K value of 0.0167 has been achieved at pH 8, which also has the highest COD removal effectiveness (97.02%). More hydroxyl radicals are

(a)

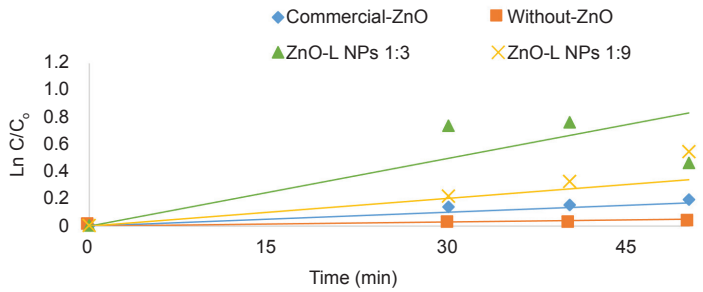

Condition	Value	
	R^2	K
Commercial ZnO	0.9621	0.0034
Without ZnO	0.7603	0.0010
ZnO-L NPs 1:3	0.9169	0.0167
ZnO-L NPs 1:9	0.8116	0.0069

(b)

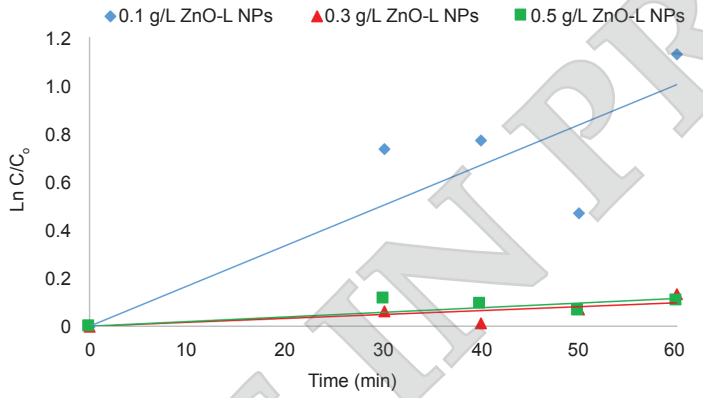

Condition	Value	
	R^2	K
0.1 g/L ZnO-L NPs	0.9172	0.0167
0.3 g/L ZnO-L NPs	0.8376	0.0016
0.5 g/L ZnO-L NPs	0.8795	0.0019

(c)

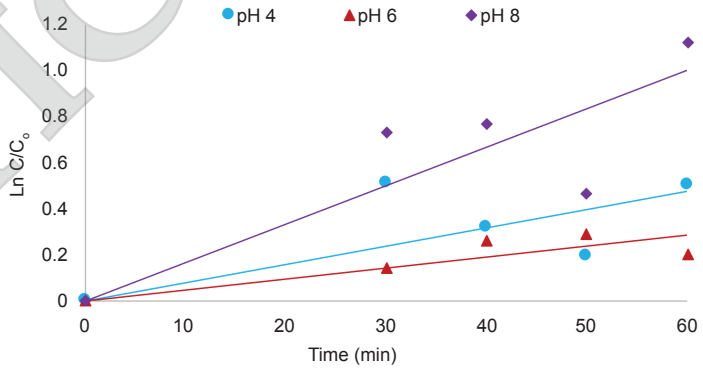

Condition	Value	
	R^2	K
pH 4	0.8254	0.0080
pH 6	0.9297	0.0048
pH 8	0.9169	0.0167

Note: The Langmuir-Hinshelwood model evaluation along with the rate constant values (K) and the correlation coefficient (R^2) for the degradation of AnT-POME.

Figure 6. Kinetic study for the degradation of AnT-POME at the different (a) types of ZnO, (b) ZnO-L loading and (c) pH of AnT-POME.

produced under basic conditions, which leads to an increase in high photocatalytic activity at higher pH. According to Chin *et al.* (2022), hydroxyl radicals are crucial in the breakdown of POME into simple compounds.

Numerous researchers are working on photocatalytic treatment. *Table 4* summarises previous studies on photocatalytic efficiency for pollutant degradation using various published photocatalysts. The removal efficiency and rate constant for the degradation of pollutants have been influenced by the photocatalyst's size. The higher particle size during the photocatalytic process may result in a lower adsorption rate, which could explain the lower degradation efficiency and first order kinetic rate (Ramesh *et al.*, 2021; Shkir *et al.*, 2024a). Most studies in *Table 4* demonstrate the impact of modified photocatalysts, which drastically reduce their size while increasing their specific surface area and photocatalytic performance. This is beneficial for UV light absorption and helps break down more contaminant molecules (Chandekar *et al.*, 2020; Shi *et al.*, 2020b; Shkir *et al.*, 2024b). Additionally, the outcomes of this investigation demonstrate that the morphological change of biosynthetic ZnO-L NPs 1:3 is attributed to the improvement of the photocatalytic performance of AnT-POME COD removal. Therefore, the specific role of biomolecule compounds in biosynthetic nanoparticles might be investigated further to show the precise mechanisms or contributions of these compounds to the material that improves photocatalyst morphology.

CONCLUSION

In conclusion, the addition of ZnO-L NPs in the photocatalytic process for treating AnT-POME improved the performance in terms of colour, turbidity and COD elimination compared to without ZnO and commercial ZnO. The findings of this investigation confirmed that AnT-POME treatment via photocatalytic process in the presence of green ZnO-L NPs 1:3 significantly improved the treated AnT-POME quality owing to the reduced size of nanoparticles (20-60 nm). The optimal photocatalyst loading for AnT-POME treatment via the photocatalytic degradation process was 0.1 g/L due to the high rate of AnT-POME particle degradation. Furthermore, water quality analysis revealed that the treated AnT-POME under the ideal photocatalyst loading (0.1 g/L) and pH (6) approaches the effluent standard as per the Environmental Quality (Prescribed Premises) (Crude Palm Oil) Regulations 1977, under the Environmental Quality Act 1974. It was discovered that the treated AnT-POME had percentages of removal for turbidity (85.62%), COD (97.02%) and colour (50.88%). As a result, it is thought that this study has a great deal of potential for use in the palm oil mill business. This study's weakness is that it has yet to be carried out on a pilot scale due to the high cost and lack of resources. Additionally, more study on the behaviour of ZnO-L NPs across a range of hues is advised to determine their adaptability and wider usefulness in a variety of real-world situations. Therefore, the results of

TABLE 4. COMPARISON OF PHOTOCATALYTIC EFFICIENCY OVER VARIOUS REPORTED PHOTOCATALYSTS FROM PREVIOUS RESEARCH

Photocatalyst	Pollutant	Removal/ Degradation efficiency (%)	Rate constant, k (min^{-1})	Size photocatalyst (nm)	Reference
LaCa	POME	54.0	0.0036	~85.0	Ghazali *et al.* (2019)
Cu @ ZnO	Methylene green	75.0-80.0	~0.0400	26.4-28.9	Chandekar *et al.* (2020)
Cu_3P–ZSO–CN p–n–n	Antibiotic	55.0-98.0	0.0543	NA	Guo *et al.* (2021)
$BiPO_4/CuBi_2O_4$	Tetracycline	92.0	0.0241	150.0-200.0	Lu *et al.* (2022)
TiO_2/RGO	Bisphenol-A	98.5	0.0009	23.0-30.0	Ramesh *et al.* (2021)
CO_5/H-CN	Tetracycline	86.0	~0.0130	NA	Shi *et al.* (2020b)
$AgPO_4/CO_3(PO_4)_2$/g-C_3N_4	Tetracycline	88.0	0.0159	40.0-100.0	Shi *et al.* (2020d)
Tb@ZnO	Methylene green	~90.0	~0.0200	NA	Shkir *et al.* (2020b)
Sr:ZnO	Methylene blue	~70.0	~0.0300	16.0-24.0	Shkir *et al.* (2020a)
Ni:ZnO	Methylene blue	94.0	0.0133	20.0-100.0	Shkir *et al.* (2022b)
$BaFe_2O_4$/BiOCl	POME	61.0	0.0045	NA	Tan *et al.* (2023)
MgO/Ag:MO	Rh-B Dye	84.0-92.0	0.0131-0.0199	21.0-28.0	Shkir *et al.* (2024a)
Ag:NiO	Methylene Blue/ Rh-B dye	88.0-99.0	0.0153-0.0309	15.0-40.0	Shkir *et al.* (2024b)
ZnO-L	AnT-POME	50.0–97.0	0.0167	20.0-60.0	This study

this study will serve as the foundation for further investigation into the photocatalytic treatment of AnT-POME on a pilot scale.

ACKNOWLEDGEMENT

This research was supported by Ministry of Higher Education (MOHE) through Fundamental Research Grant Scheme (FRGS/1/2023/TK08/UTHM/02/3) (K477). Research Grant Tier 1 (Q439) from Universiti Tun Hussein Onn Malaysia provided funding for this study. The Centre for Diploma Studies at Universiti Tun Hussein Onn Malaysia is also acknowledged by the authors for its support.

REFERENCES

Agarwal, H., Kumar, S. V., & Rajeshkumar, S. (2017). A review on green synthesis of zinc oxide nanoparticles – An eco-friendly approach. *Resource-Efficient Technologies*, *3*(4), 406–413. https://doi.org/10.1016/j.reffit.2017.03.002

Ajayi, E., & Afolayan, A. (2017). Green synthesis, characterization and biological activities of silver nanoparticles from alkalinized *Cymbopogon citratus* Stapf. *Advances in Natural Sciences Nanoscience and Nanotechnology*, *8*(1), 015017. https://doi.org/10.1088/2043-6254/aa5cf7

Alagarasan, D., Hegde, S., Naik, R., Murahari, P., Shetty, H. D., Hb, S. P., Maiz, F., & Shkir, M. (2024). Fabrication of high-performance RT-NH_3 gas sensor based on Cu and La co-doped ZnO films through a facile drop-casting method. *Optical Materials*, *147*, 114705. https://doi.org/10.1016/j.optmat.2023.114705

Awang, Z., Hairom, N. H. H., Hamid, N. H. A., Sidik, D. A. B., Nadzim, U. K. H. M., Madon, R. H., & Yong, N. L. (2024). Palm oil mill secondary effluent treatment using ZNO-clay liquid photocatalyst in membrane photocatalytic reactor. *Journal of the Indian Chemical Society*, *101*(7), 101158. https://doi.org/10.1016/j.jics.2024.101158

Bello, M. M., & Raman, A. A. A. (2017). Trend and current practices of palm oil mill effluent polishing: Application of advanced oxidation processes and their future perspectives. *Journal of Environmental Management*, *198*, 170–182. https://doi.org/10.1016/j.jenvman.2017.04.050

Cao, S., Zhu, R., Wu, D., Su, H., Liu, Z., & Chen, Z. (2024). How hydrogen bonding and π–π interactions synergistically facilitate mephedrone adsorption by bio-sorbent: An in-depth microscopic scale interpretation. *Environmental Pollution*, *342*, 123044. https://doi.org/10.1016/j.envpol.2023.123044

Chan, J. S., Low, M., Poh, P. E., Yeo, L. Y., & Tan, M. K. (2023). Palm oil mill effluent processing via hybrid plasma and acoustic treatment. *Journal of Water Process Engineering*, *51*, 103455. https://doi.org/10.1016/j.jwpe.2022.103455

Chandekar, K. V., Shkir, M., Al-Shehri, B. M., AlFaify, S., Halor, R. G., Khan, A., Al-Namshah, K. S., & Hamdy, M. S. (2020). Visible light sensitive Cu doped ZnO: Facile synthesis, characterization and high photocatalytic response. *Materials Characterization*, *165*, 110387. https://doi.org/10.1016/j.matchar.2020.110387

Chin, Y., Sin, J., Lam, S., Zeng, H., Lin, H., Li, H., & Mohamed, A. R. (2022). 0-D/3-D heterojunction composite constructed by decorating transition metal oxide nanoparticle on peony-like ZnO hierarchical microstructure for improved photodegradation of palm oil mill effluent. *Optik*, *260*, 169098. https://doi.org/10.1016/j.ijleo.2022.169098

Desa, A. L., Hairom, N. H. H., Sidik, D. A. B., Zainuri, N. Z., Ng, L. Y., Mohammad, A. W., Jusoh, N. W. C., & Jalil, A. A. (2020). Performance of tight ultrafiltration membrane in textile wastewater treatment via MPR system: Effect of pressure on membrane fouling. *IOP Conference Series Materials Science and Engineering*, *736*(2), 022033. https://doi.org/10.1088/1757-899x/736/2/022033

Devi, T. B., Begum, S., & Ahmaruzzaman, M. (2016). Photo-catalytic activity of Plasmonic Ag@AgCl nanoparticles (synthesized via a green route) for the effective degradation of Victoria Blue B from aqueous phase. *Journal of Photochemistry and Photobiology B Biology*, *160*, 260–270. https://doi.org/10.1016/j.jphotobiol.2016.03.033

Ghazali, S. S., Jusoh, R., & Shariffuddin, J. H. (2019). Parameter affecting photocatalytic degradation of POME using LaCa as photocatalyst. *Materials Today Proceedings*, *19*, 1173–1182. https://doi.org/10.1016/j.matpr.2019.11.120

Guo, F., Huang, X., Chen, Z., Cao, L., Cheng, X., Chen, L., & Shi, W. (2021). Construction of Cu_3P-$ZnSnO_3$-g-C_3N_4 p-n-n heterojunction with multiple built-in electric fields for effectively boosting visible-light photocatalytic degradation of broad-spectrum antibiotics. *Separation and*

Purification Technology, *265*, 118477. https://doi.org/10.1016/j.seppur.2021.118477

Hairom, N. H. H., Mohammad, A. W., Ng, L. Y., & Kadhum, A. A. H. (2015). Utilization of self-synthesized ZnO nanoparticles in MPR for industrial dye wastewater treatment using NF and UF membrane. *Desalination and Water Treatment*, *54*(4–5), 944–955. https://doi.org/10.1080/19443994.2014.917988

Jansi, R., Revathy, Juliet, A. V., Manthrammel, M. A., & Shkir, M. (2024). High response chemiresistive room temperature ammonia gas sensor based on La-doped ZnO samples. *Ceramics International*, *50*(17), 29419–29427. https://doi.org/10.1016/j.ceramint.2024.05.236

Khan, Z., Alshammari, A. S., & Shkir, M. (2024). Role of Zn doping in improving opto-nonlinear and photodetection properties of spray pyrolysis grown $Cd_{1-x}Zn_xS$ nanostructured thin films. *Radiation Physics and Chemistry*, *216*, 111382. https://doi.org/10.1016/j.radphyschem.2023.111382

Lim, K. S., Sethu, V., & Selvarajoo, A. (2022). Natural plant materials as coagulant and flocculants for the treatment of palm oil mill effluent. *Materials Today Proceedings*, *48*, 871–887. https://doi.org/10.1016/j.matpr.2021.02.483

Lu, C., Wang, L., Yang, D., Jin, Z., Wang, X., Xu, J., Li, Z., Shi, W., Guan, W., & Huang, W. (2022). Boosted tetracycline and Cr(VI) simultaneous cleanup over Z-Scheme $BiPO_4/CuBi_2O_4$ p-n heterojunction with 0D/1D trepang-like structure under simulated sunlight irradiation. *Journal of Alloys and Compounds*, *919*, 165849. https://doi.org/10.1016/j.jallcom.2022.165849

Mohamad, N. A., Hamzah, S., Harun, M. H. C., Ali, A., Rasit, N., Awang, M., Rahman, W. R. W. A., Azmi, A. A. A. R., Habib, A. A., Zahid, M. S. A., Mustofa, A. A. F., Latfi, S. A., Aripin, S. M., & Saad, R. (2021). Integration of copperas and calcium hydroxide as a chemical coagulant and coagulant aid for efficient treatment of palm oil mill effluent. *Chemosphere*, *281*, 130873. https://doi.org/10.1016/j.chemosphere.2021.130873

Mohamad, Z., Razak, A. A., Krishnan, S., Singh, L., Zularisam, A., & Nasrullah, M. (2022). Treatment of palm oil mill effluent using electrocoagulation powered by direct photovoltaic solar system. *Process Safety and Environmental Protection*, *177*, 578–582. https://doi.org/10.1016/j.cherd.2021.11.019

Moksin, N. S. A., Ong, Y. P., Ho, L., & Tay, M. G. (2021). Optimization of photocatalytic fuel cells (PFCs) in the treatment of diluted palm oil mill effluent (POME). *Journal of Water Process Engineering*, *40*, 101880. https://doi.org/10.1016/j.jwpe.2020.101880

Muhamad, N., Mokhtar, N., Lau, W., Ismail, A., & Naim, R. (2022). Fouling studies on hydrophobic PVDF-bentonite hollow fiber membrane during membrane distillation of palm oil mill effluent. *Journal of Water Process Engineering*, *49*, 102969. https://doi.org/10.1016/j.jwpe.2022.102969

Nawaz, R., Kait, C. F., Chia, H. Y., Isa, M. H., & Huei, L. W. (2020). Photocatalytic remediation of treated palm oil mill effluent contaminated with phenolic compounds using TiO_2 nanomaterial. *Desalination and Water Treatment*, *183*, 355–365. https://doi.org/10.5004/dwt.2020.25218

Ng, K. H., Yuan, L. S., Cheng, C. K., Chen, K., & Fang, C. (2019). TiO_2 and ZnO photocatalytic treatment of palm oil mill effluent (POME) and feasibility of renewable energy generation: A short review. *Journal of Cleaner Production*, *233*, 209–225. https://doi.org/10.1016/j.jclepro.2019.06.044

Puasa, N. A., Hairom, N. H. H., Dzinun, H., Madon, R. H., Ahmad, N. S., Sidik, D. A. B., & Azmi, A. A. A. R. (2021). Photocatalytic degradation of palm oil mill secondary effluent in presence of zinc oxide nanoparticles. *Environmental Nanotechnology Monitoring & Management*, *15*, 100413. https://doi.org/10.1016/j.enmm.2020.100413

Ramesh, K., Gnanavel, B., & Shkir, M. (2021). Enhanced visible light photocatalytic degradation of bisphenol A (BPA) by reduced graphene oxide (RGO)-metal oxide (TiO_2, ZnO and WO_3) based nanocomposites. *Diamond and Related Materials*, *118*, 108514. https://doi.org/10.1016/j.diamond.2021.108514

Rao, K. J., Kumaravel, V., Pownraj, I., Saha, K., Korumilli, T., & Sadasivam, S. K. (2022). Biosynthesis and photocatalytic evaluation of ZnO nanoparticles using banana flower perianth. *Journal of Cleaner Production*, *380*, 135180. https://doi.org/10.1016/j.jclepro.2022.135180

Razali, N. A. M., Salleh, W. N. W., Rosman, N., Ismail, N. H., Ahmad, S. Z. N., Aziz, F., Jye, L. W., & Ismail, A. F. (2021). Palm oil mill effluent

treatment using tungsten trioxide: Adsorption and photocatalytic degradation. *Materials Today Proceedings*, *42*, 22–27. https://doi.org/10.1016/j.matpr.2020.08.424

Ren, X., Chen, R., Ding, S., & Fu, N. (2023). Preparation and photocatalytic performance of a magnetically recyclable $ZnFe_2O_4$@TiO_2@Ag_2O p-n/Z-type tandem heterojunction photocatalyst: Degradation pathway and mechanism. *Colloids and Surfaces A: Physicochemical and Engineering Aspects*, *658*, 130604. https://doi.org/10.1016/j.colsurfa.2022.130604

Sayadi, M. H., Ghollasimood, S., Ahmadpour, N., & Homaeigohar, S. (2022). Biosynthesis of the ZnO/SnO_2 nanoparticles and characterization of their photocatalytic potential for removal of organic water pollutants. *Journal of Photochemistry and Photobiology A: Chemistry*, *425*, 113662. https://doi.org/10.1016/j.jphotochem.2021.113662

Sayuti, S. C., & Azoddein, A. A. M. (2015). Treatment of palm oil mill effluent (POME) by using electrocoagulation as an alternative method. *Malaysian Journal of Analytical Sciences*, *19*(4), 663–668.

Schnabel, T., Dutschke, M., Schuetz, F., Hauser, F., & Springer, C. (2022). Photocatalytic air purification of polycyclic aromatic hydrocarbons: Application of a flow-through reactor, kinetic studies and degradation pathways. *Journal of Photochemistry and Photobiology A: Chemistry*, *430*, 113993. https://doi.org/10.1016/j.jphotochem.2022.113993

Shi, W., Li, M., Huang, X., Ren, H., Yan, C., & Guo, F. (2020a). Facile synthesis of 2D/2D $Co_3(PO_4)_2$/g-C_3N_4 heterojunction for highly photocatalytic overall water splitting under visible light. *Chemical Engineering Journal*, *382*, 122960. https://doi.org/10.1016/j.cej.2019.122960

Shi, W., Liu, C., Li, M., Lin, X., Guo, F., & Shi, J. (2020b). Fabrication of ternary Ag_3PO_4/$Co_3(PO_4)_2$/g-C_3N_4 heterostructure with following Type II and Z-Scheme dual pathways for enhanced visible-light photocatalytic activity. *Journal of Hazardous Materials*, *389*, 121907. https://doi.org/10.1016/j.jhazmat.2019.121907

Shi, W., Shu, K., Sun, H., Ren, H., Li, M., Chen, F., & Guo, F. (2020c). Dual enhancement of capturing photogenerated electrons by loading CoP nanoparticles on N-deficient graphitic carbon nitride for efficient photocatalytic degradation of tetracycline under visible light. *Separation and Purification Technology*, *246*, 116930. https://doi.org/10.1016/j.seppur.2020.116930

Shi, W., Yang, S., Sun, H., Wang, J., Lin, X., Guo, F., & Shi, J. (2020d). Carbon dots anchored high-crystalline g-C_3N_4 as a metal-free composite photocatalyst for boosted photocatalytic degradation of tetracycline under visible light. *Journal of Materials Science*, *56*(3), 2226–2240. https://doi.org/10.1007/s10853-020-05436-2

Shkir, M. (2022a). Green method for synthesis and characterization of copper oxide nanoparticles using mulberry plant extract and their antibacterial, antioxidant and photocatalytic activity. *Physica Scripta*, *97*(10), 105001. https://doi.org/10.1088/1402-4896/ac8a7a

Shkir, M., AlAbdulaal, T., Manthrammel, M. A., & Khan, F. S. (2024a). Novel MgO and Ag/MgO nanoparticles green-synthesis for antibacterial and photocatalytic applications: A kinetics-mechanism & recyclability. *Journal of Photochemistry and Photobiology A: Chemistry*, *449*, 115398. https://doi.org/10.1016/j.jphotochem.2023.115398

Shkir, M., Al-Shehri, B. M., Pachamuthu, M., Khan, A., Chandekar, K. V., AlFaify, S., & Hamdy, M. S. (2020a). A remarkable improvement in photocatalytic activity of ZnO nanoparticles through Sr doping synthesized by one pot flash combustion technique for water treatments. *Colloids and Surfaces A: Physicochemical and Engineering Aspects*, *587*, 124340. https://doi.org/10.1016/j.colsurfa.2019.124340

Shkir, M., Baskaran, P., Khan, A., & Khan, M. T. (2024b). Remarkable improvement in photocatalytic activity of NiO nanoparticles through Ag doping: A kinetics-mechanism & recyclability. *International Journal of Hydrogen Energy*, *73*, 54–62. https://doi.org/10.1016/j.ijhydene.2024.05.466

Shkir, M., Chandekar, K. V., Alshehri, B. M., Khan, A., AlFaify, S., & Hamdy, M. S. (2020b). A remarkable enhancement in photocatalytic activity of facilely synthesized Terbium@Zinc oxide nanoparticles by flash combustion route for optoelectronic applications. *Applied Nanoscience*, *10*(6), 1811–1823. https://doi.org/10.1007/s13204-019-01236-6

Shkir, M., Khan, M. T., & Khan, A. (2024c). Impact of Mo doping on photo-sensing properties of ZnO thin films for advanced photodetection

applications. *Journal of Alloys and Compounds*, *985*, 174009. https://doi.org/10.1016/j.jallcom.2024.174009

Shkir, M., Khan, M. T., Khan, A., Alkallas, F., Trabelsi, A. B. G., Khan, F. S., & AlFaify, S. (2024d). Noticeable influence of V-dopant on optoelectronic properties of ZnO films prepared by SILAR technique. *Results in Physics*, *60*, 107680. https://doi.org/10.1016/j.rinp.2024.107680

Shkir, M., Palanivel, B., Khan, A., Kumar, M., Chang, J., Mani, A., & AlFaify, S. (2022b). Enhanced photocatalytic activities of facile auto-combustion synthesized ZnO nanoparticles for wastewater treatment: An impact of Ni doping. *Chemosphere, 291*, 132687. https://doi.org/10.1016/j.chemosphere.2021.132687

Sidhu, A. K., Verma, N., & Kaushal, P. (2022). Role of biogenic capping agents in the synthesis of metallic nanoparticles and evaluation of their therapeutic potential. *Frontiers in Nanotechnology*, *3*, 801620. https://doi.org/10.3389/fnano.2021.801620

Sidik, D. A. B., Hairom, N. H. H., Ahmad, M. K., Madon, R. H., & Mohammad, A. W. (2020). Performance of membrane photocatalytic reactor incorporated with ZnO-*Cymbopogon citratus* in treating palm oil mill secondary effluent. *Process Safety and Environmental Protection*, *143*, 273–284. https://doi.org/10.1016/j.psep.2020.06.038

Som, A. M., & Yahya, A. (2021). Kinetics and performance study of ultrasonic-assisted membrane anaerobic system using Monod Model for palm oil mill effluent (POME) treatment. *Cleaner Engineering and Technology*, *2*, 100075. https://doi.org/10.1016/j.clet.2021.100075

Tan, J., Sin, J., Lam, S., Lin, H., Li, H., Huang, L., & Mohamed, A. R. (2023). Fabrication of novel Z-scheme $BaFe_2O_4$/BiOCl nanocomposite with promoted visible light photocatalytic palm oil mill effluent treatment and pathogens destruction. *Inorganic Chemistry Communications*, *152*, 110659. https://doi.org/10.1016/j.inoche.2023.110659

Zainuri, N. Z., Hairom, N. H. H., Sidik, D. A. B., Desa, A. L., Misdan, N., Yusof, N., & Mohammad, A. W. (2018). Palm oil mill secondary effluent (POMSE) treatment via photocatalysis process in presence of ZnO-PEG nanoparticles. *Journal of Water Process Engineering*, *26*, 10–16. https://doi.org/10.1016/j.jwpe.2018.08.009